Journal of Marine Research, 54, 451–469, 1996

Application of a barotropic model to North Atlantic synoptic sea level variability

by Richard J. Greatbatch[1], Youyu Lu[1,2], and Brad de Young[1]

ABSTRACT

A barotropic, shallow-water model of the North Atlantic is used to investigate variability in adjusted sea level on time scales of a few days to a few months (by "adjusted," we mean that the inverse barometer is removed from both the model-computed sea level and the observations). The model has ⅓° × 0.4° resolution in latitude and longitude, respectively, and is forced using atmospheric pressure and wind stress data derived from European Centre for Medium Range Weather Forecasts (ECMWF, 1994) analyses. The model results are compared with coastal tide gauge data. Along the western boundary, from St. John's, Newfoundland, to Fernandina Beach, Florida, coherence squared between model and data is greater than 0.5 in the period range 3 to 10 days. South of Cape Hatteras, the model underestimates the amplitude seen in the data, with much better agreement north of the Cape. Model performance on the eastern boundary is generally poor. We suggest this is because on the eastern boundary, the shelf width is much narrower, compared to the internal radius of deformation, than on the western boundary. In addition, the model resolution is insufficient to adequately represent the shelf on the eastern boundary. The poorer agreement south of Cape Hatteras may be due Gulf Stream effects not accounted for by the model dynamics. Finally, we discuss the model-computed variability in the ocean interior.

1. Introduction

We investigate the ability of a barotropic, shallow-water model to account for North Atlantic coastal sea level variability at time scales of a few days to seasonal. The model is driven by surface forcing derived from atmospheric data for the years 1985 and 1986. In previous work, we showed the model has skill in accounting for bottom pressure variability on the Labrador and Newfoundland shelves (de Young *et al.,* 1995), and transport variability through the Straits of Florida (Greatbatch *et al.,* 1995). It is natural to ask if the model exhibits similar skill with coastal sea level. The study is topical because of an ongoing nowcast/forecast system being developed for the continental shelf/slope region along the east coast of North America (Mellor, personal communication, 1994, Aikmann *et al.,* 1994). Coastal sea level provides an

1. Department of Physics, Memorial University of Newfoundland, St. John's, Newfoundland, Canada A1B 3X7.

2. Present address: School of Earth and Ocean Sciences, University of Victoria, British Columbia, Canada, V8W 2Y2.

important source of data for this enterprise. As such, it is important to understand those processes that influence coastal sea level, and also the ability of simpler models, such as those we describe, to account for the observed variability. In addition, the availability of satellite altimeter data, in particular from TOPEX/POSEIDON, has stimulated much recent interest in sea level studies, and the assimilation of altimetric data into ocean models (see Fu *et al.,* 1994, and the other articles in that journal issue on TOPEX/POSEIDON). Consistency between Geosat altimeric data and coastal tide gauge data has been demonstrated by Wunsch (1991a), at least on large space scales (several thousand kilometers), and time scales from several months to two years. He has also shown that a large part of the observed sea level variability, on the same space and time scales, appears to be related to wind and atmospheric pressure forcing (Wunsch, 1991b).

In the North Atlantic, much of the interest in sea level studies has been focused on the western Atlantic. Studies have examined the mean alongshore gradient (Sturges, 1974; Blaha and Sturges, 1987; Ezer and Mellor, 1994), and the variability of sea level on time scales of days and months (Noble and Butman, 1979; Chase, 1979; Wang, 1979; Sandstrom, 1980), to interannual and interdecadal (Thompson, 1986; Ezer *et al.*, 1995). Noble and Butman (1979) showed that wind stress and adjusted sea level are coherent on length scales of 1300 km at periods between 60 and 600 hours. Wang (1979) found somewhat shorter coherence length scales south of Cape Cod, with evidence of free wave phase propagation of 600 km/day. Blaha (1984) discusses the influence of variations in the Gulf Stream on the seasonal variation of sea level in the South Atlantic Bight. This issue was also addressed by Greatbatch and Goulding (1989a) using a coarse resolution, barotropic model of the North Atlantic. At seasonal time scales, sea level is strongly influenced by steric effects (Pattullo *et al.,* 1955). Greatbatch and Goulding (1989a) tried removing the steric effect from tide gauge data to enable comparison with their model. In general, they found much better agreement between model and data along the western than the eastern boundary. A later paper (Greatbatch *et al.,* 1990) successfully used a barotropic model to separate the influence of North Atlantic wind forcing from local wind forcing on the seasonal variation of sea level on the Newfoundland and Labrador Shelf, verifying an empirical analysis by Thompson *et al.* (1986).

The work in this paper extends that of Greatbatch and Goulding (1989a) and Greatbatch *et al.* (1990), by concentrating on synoptic time scales of days to months, by using a model with much higher resolution, and by including atmospheric pressure in addition to wind stress forcing. Wunsch (1972) and Ponte *et al.* (1991) have argued that the inverse barometer should be a valid approximation on time scales greater than about two days, yet significant departures from the inverse barometer have been observed on the Labrador Shelf at time scales of two to ten days (Garrett *et al.,* 1985; Wright *et al.,* 1987), and are a feature of the model solutions of de Young *et al.* (1995). In the next section we describe the model, followed by presentation of the

tide gauge data in Section 3. The model results are compared with the data in Section 4, and in Section 5, we conclude with a summary.

2. Model

In previous studies of North Atlantic synoptic and seasonal variability, we applied a barotropic stream function model which had a rigid-lid and was solved in the frequency domain (Greatbatch and Goulding, 1989a; Greatbatch *et al.*, 1990; de Young *et al.*, 1992). While successful, particularly in elucidating the seasonal signal, we now relax the rigid-lid condition and include atmospheric pressure forcing.

The model is based on the vertically-integrated, shallow-water equations for a homogeneous ocean, linearized about a state of rest (Gill, 1982), and is forced by wind stress and atmospheric pressure. In spherical coordinates the governing equations are

$$\frac{\partial \eta}{\partial t} + \frac{1}{a \cos \phi}\left[\frac{\partial}{\partial \lambda}(Hu) + \frac{\partial}{\partial \phi}(Hv \cos \phi)\right] = 0 \tag{1}$$

$$\frac{\partial u}{\partial t} - 2\Omega \sin \phi v = -\frac{g}{a \cos \phi}\frac{\partial}{\partial \lambda}\left(\eta + \frac{p_a}{\rho_o g}\right) + \frac{\tau_s^\lambda - \tau_b^\lambda}{\rho_o H} + A_h f^\lambda \tag{2}$$

$$\frac{\partial v}{\partial t} + 2\Omega \sin \phi u = -\frac{g}{a}\frac{\partial}{\partial \phi}\left(\eta + \frac{p_a}{\rho_o g}\right) + \frac{\tau_s^\phi - \tau_b^\phi}{\rho_o H} + A_h f^\phi \tag{3}$$

where η is the upward displacement of sea level, a is the radius of the earth, ϕ is the latitude, λ is the longitude, H is the water depth, u and v are the eastward and northward components of velocity, A_h is the horizontal eddy viscosity, Ω is the rotation rate of the earth, g the acceleration due to gravity, p_a is the atmospheric pressure, and ρ_o is a representative density for sea water (here 1025 kg m^{-3}). τ_s^λ and τ_s^ϕ are the eastward and northward components of the surface wind stress. τ_b^λ and τ_b^ϕ are the components of bottom stress which are related to the velocity field by a quadratic bottom friction law

$$(\tau_b^\lambda, \tau_b^\phi)/\rho_o = k(u^2 + v^2)^{1/2}(u, v)$$

k is the empirical quadratic bottom friction coefficient. Lateral mixing is parameterized following Bryan (1969)

$$f^\lambda = \frac{1}{a^2 \cos^2 \phi}\frac{\partial^2 u}{\partial \lambda^2} + \frac{1}{a^2 \cos \phi}\frac{\partial}{\partial \phi}\left(\cos \phi \frac{\partial u}{\partial \phi}\right) + \frac{1}{a^2}\left[(1 - \tan^2 \phi)u - \frac{2 \tan \phi}{\cos \phi}\frac{\partial v}{\partial \lambda}\right] \tag{4}$$

$$f^\phi = \frac{1}{a^2 \cos^2 \phi}\frac{\partial^2 v}{\partial \lambda^2} + \frac{1}{a^2 \cos \phi}\frac{\partial}{\partial \phi}\left(\cos \phi \frac{\partial v}{\partial \phi}\right) + \frac{1}{a^2}\left[(1 - \tan^2 \phi)v + \frac{2 \tan \phi}{\cos \phi}\frac{\partial u}{\partial \lambda}\right]. \tag{5}$$

To solve these equations we use the finite difference method described by Heaps

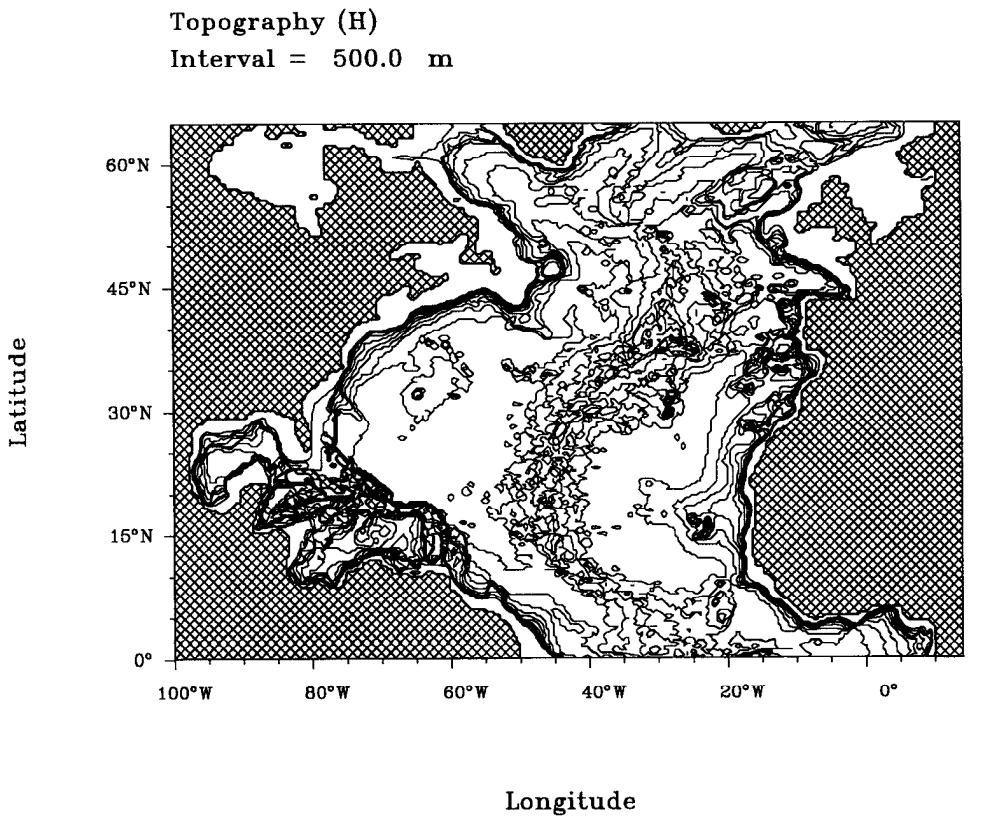

Figure 1 (a) Bottom topography used in the model. The contour interval is 500 m. (b) Location of the stations discussed in this analysis (see Table 1). (1) St. John's (2) Halifax (3) Portland (4) Atlantic City (5) Hampton Roads (6) Charleston (7) Fort Pulaski (8) Fernandina Beach (9) Haulover Pier (10) Reykjavik (11) Newlyn (12) Brest (13) La Coruna (14) Lagos (15) Las Palmas.

(1971). In particular, the spatial differential operators are calculated using centered differencing on the C-grid. Forward-time differencing is applied to (1), and backward differencing to (2) and (3), except for the Coriolis term in (2) which is calculated using forward-time differencing. The lateral and bottom friction terms are treated explicitly. The bottom topography is the same as that used by Bryan and Holland (1989) in an eddy-resolving general circulation model of the North Atlantic, except that we close the model domain at the equator, and the Hudson Bay—Hudson Strait system is included (Fig. 1a). The resolution is $\frac{1}{3}°$ in latitude and $\frac{2}{5}°$ in longitude, giving an equal grid spacing in the north-south and east-west directions of about 37 km at 34N. The topography is stepwise (with 30 discrete depth levels). A "no-slip" boundary condition is applied along the coastal boundaries, and also along the

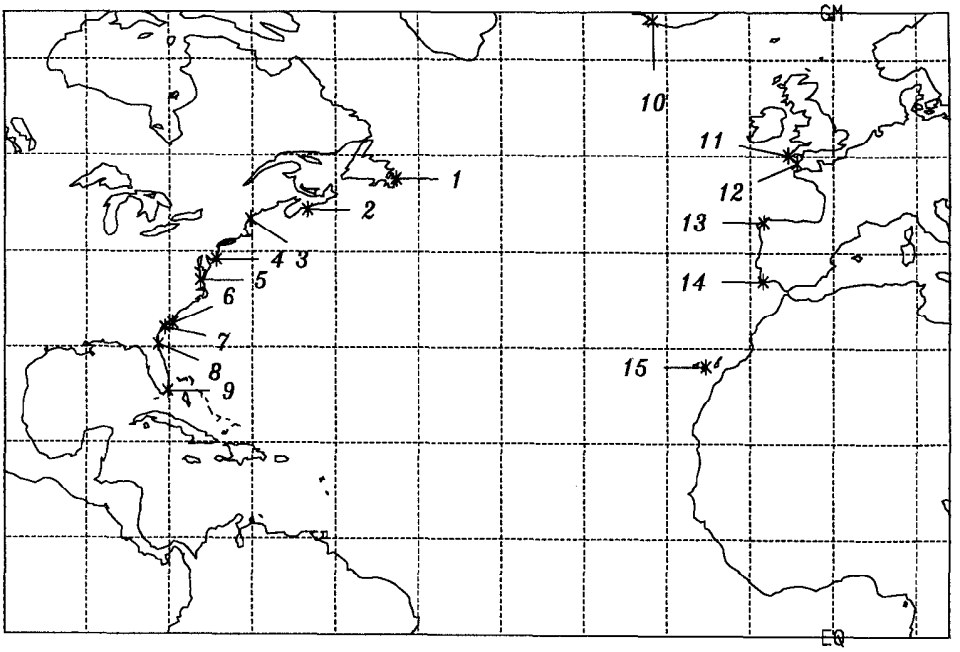

Figure 1. (Continued)

northern and southern boundaries of the model domain (i.e. at the equator, and 65N).

The surface pressure and 10 m wind fields used to drive the model are twice daily analyses (0000 and 1200 GMT) from the European Centre for Medium Range Weather Forecasts (ECMWF) for the years 1985 and 1986, taken from the TOGA/WCRP Level III Basic Data Set (European Centre for Medium Range Weather Forecasts, 1994). The wind and atmospheric pressure fields are interpolated to the model grid using the interpolation scheme of Akima (1978). The wind stress is then calculated using the formula of Large and Pond (1981), and the forcing fields linearly interpolated in time to the model time step. The impact of missing data and changes in the ECMWF analysis procedure during the years 1985 and 1986 will be addressed when we discuss the model results in Section 4.

In the model runs to be described, the quadratic bottom friction and horizontal eddy viscosity coefficients have values $k = 2.5 \times 10^{-3}$ and $A_h = 10^3$ m^2 s^{-1}, respectively. These values of k and A_h reproduce the correct pattern of amphidromic points under tidal forcing, suggesting their appropriateness for our study. Sensitivity tests show that the model results are not strongly dependent upon the value of A_h. The model is initialized with $u = v = \eta = 0$ at 0000 GMT on January 1, 1985. After about three weeks integration, the model has forgotten its initial condition.

A major contributor to observed (and model-computed) sea level is given by the

Table 1. The tide gauge stations used in this study. The station number in the first column can be used to identify the stations in Figure 1b.

Station Number	Station Name	Latitude	Longitude
1	St. John's, NF	47.57	52.68
2	Halifax, N.S.	44.38	63.35
3	Portland, ME	43.41	70.18
4	Atlantic City, NJ	39.21	74.29
5	Hampton Roads, VA	37.02	76.23
6	Charleston, SC	32.48	79.58
7	Fort Pulaski, GA	32.03	80.54
8	Fernandina Beach, FL	30.30	81.26
9	Haulover Pier, FL	25.75	80.25
10	Reykjavik, Iceland	64.09	21.58
11	Newlyn, Britain	50.06	5.34
12	Brest, France	49.23	4.30
13	La Coruna, Spain	43.22	8.24
14	Lagos, Portugal	37.05	8.40
15	Las Palmas, Spain	28.08	15.27

inverse barometer (Gill, 1982). The inverse barometer contribution is dynamically unimportant, and it is necessary to remove it from both the observed sea level and from the model-computed sea level in order to make meaningful comparisons. In keeping with common usage, sea level from which the inverse barometer has been removed will be referred to as "adjusted sea level." In defining the inverse barometer, account must be taken of the fact that our model domain covers only the North Atlantic, and not the global ocean. For this reason, the inverse barometer (hereafter referred to as IB) is given by

$$-\eta_a = \frac{1}{\rho_o g}(p_a - \overline{p_a})$$

where, in the case of the model, $\overline{p_a}$ is the area-averaged, surface atmospheric pressure over the model domain, and in the case of the tide gauge data, $\overline{p_a}$ is the area-average of surface atmospheric pressure over the global ocean.

3. North Atlantic tide gauge data

Appropriate tide gauge data required for this study were difficult to obtain. We required long time series, but needed a sampling period short enough to allow us to remove tidal energy, yet retain energy at synoptic periods. Data for the 15 stations shown in Figure 1b were obtained from the Marine Environmental Data Service (Ottawa) for the years 1985 and 1986. (The detailed locations of these stations are given in Table 1.) Harmonic analysis was performed on the hourly data and the time series were then detided (Godin, 1972). The data were then sampled at six hour

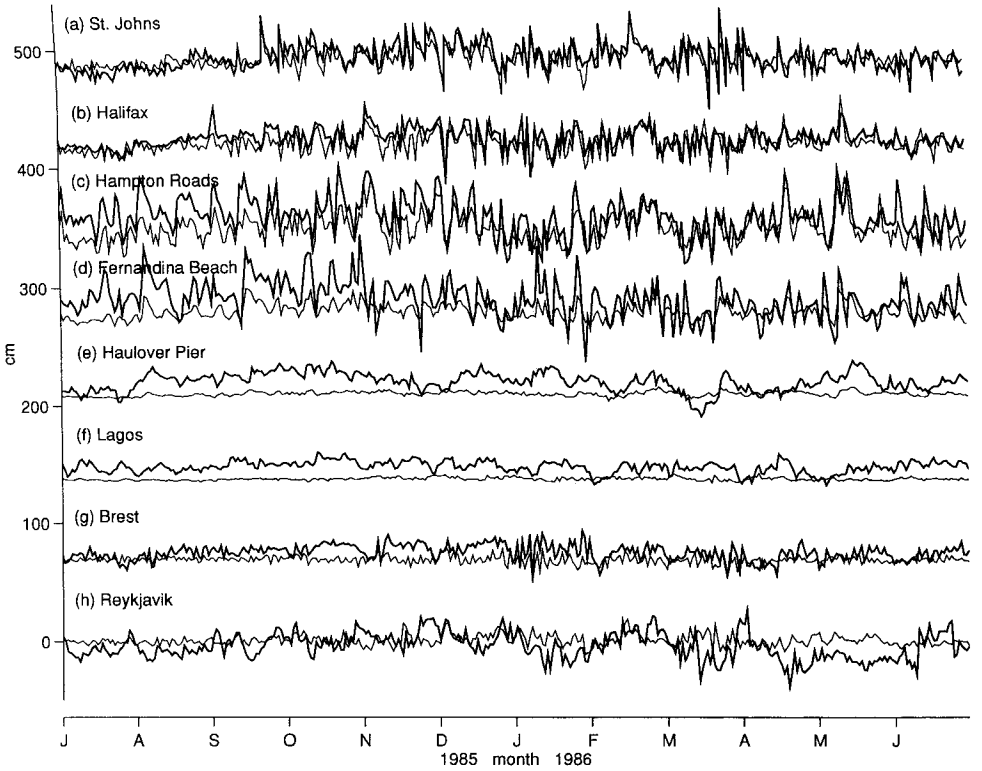

Figure 2. Time series of adjusted sea level (in cm) at (a) St. John's, (b) Halifax, (c) Hampton Roads, (d) Fernandina Beach, (e) Haulover Pier, (f) Lagos, (g) Brest, (h) Reykjavik. The observed data (the heavy line) have the tides removed, are subsampled to a six-hour sample interval, and are then low-passed filtered with a cut-off of two days. The thin line indicates the model results. Each successive time series is offset by 70 cm for ease of comparison.

intervals, the IB removed, and a low-pass filter applied with a cutoff period of two days to remove any residual energy at periods shorter than approximately 36 hours.

Sample resultant time series are shown by the heavy solid lines in Figure 2. The strongest difference between seasons is apparent at high latitudes, with St. John's and Halifax exhibiting substantially lower variance in summer than in winter. In summer, there is greater variance south of Cape Hatteras than farther north, something that may be due to the presence of the Gulf Stream (although the model results, shown by the thin solid line, show similar behavior, but with reduced amplitude, despite the absence of the Gulf Stream from the model). On the eastern boundary, the variance increases from south to north, but with generally less variance than on the western boundary. There is also a clear change in the character of the records on the western side of the basin between Fernandina Beach, Florida, and Haulover Pier, Miami, something that can also be seen in Thompson (1986).

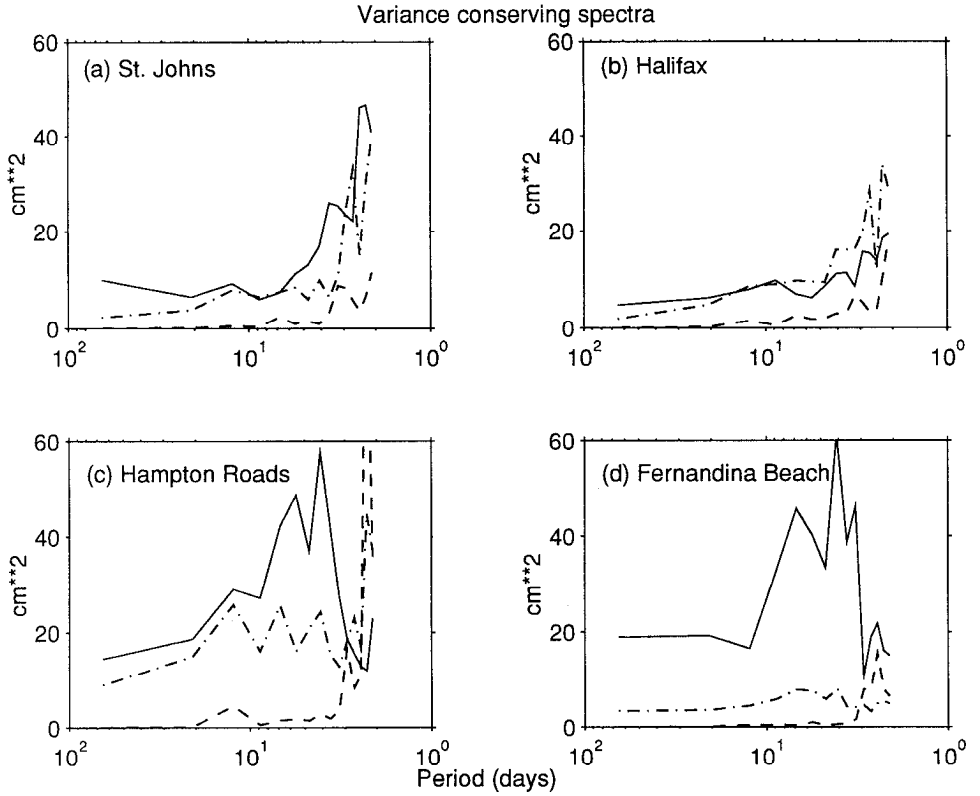

Figure 3. Variance preserving autospectra for (a) St. John's, (b) Halifax, (c) Hampton Roads and (d) Fernandina Beach. The observed data are given by the solid line. The dot-dashed line shows the model results in the wind and pressure forced case, the dashed line shows the results from the model forced by pressure only.

Variance- preserving spectra reveal substantial differences in the frequency distribution of the energy at the different observation sites (the solid lines in Fig. 3). At Halifax and St. John's the peak in energy is close to the cutoff period of the filter, between two and six days. To the south, at Hampton Roads and Fernandina Beach, the peak energy is at longer periods, from four to ten days, with a maximum near seven days. To some extent this shift can be seen in the model results (thin solid lines), which we discuss in detail in the next section.

A feature of the data worth noting is that some events in Figure 2a occur at all stations, or at groups of stations. For example, there is an event at the end of January 1986 that is found at all stations along the western boundary, except Haulover Pier, with amplitude increasing southward. Another event at the end of October 1985 is found at St. John's, Halifax and Hampton Roads, but not at Fernandina Beach. Interestingly, the model results (thin solid line) also capture these events, with generally similar characteristics.

4. Model results

Two basic model experiments were carried out: (i) pressure and wind forcing combined, and (ii) pressure forcing only. The thin line in Figure 2 shows results from the experiment with pressure and wind forcing (this is adjusted sea level, sampled daily and low-pass filtered with a cut-off of two days). It is clear that on the western boundary, the model performs quite well, with particularly good agreement at the two northern stations. Farther south, the model captures most of the events in the observations, but increasingly underpredicts the amplitude as one moves southward. The exception is Haulover Pier, where the model performance is poor. The model also performs badly at all the stations on the eastern boundary, although at Brest and Newlyn (not shown), some events are captured. At Reykjavik, the comparison between model and observations is probably not very meaningful, given that the station is on the artificially closed northern boundary of the model domain. We suggest that the weaker performance of the model on the eastern, compared to the western boundary, is because of the much narrower shelf on the eastern side, as discussed in detail in the next paragraph. It is interesting to note that what agreement there is on the eastern boundary occurs where the shelf width becomes comparable to that on the western side (at Brest and Newlyn), and also that the comparison between model and observations is worst on the western boundary at Haulover, where the shelf width is considerably narrower than farther north. Interestingly, the poor agreement at Haulover is found despite the skill of the model in capturing transport variations in the offshore Florida Current at the same time scales (Greatbatch *et al.,* 1995). This could be because of the importance of baroclinic effects in determining sea level variations at Haulover Pier (Maul *et al.,* 1990), although it could also be a consequence of inadequate model resolution, as discussed below. Figure 4 shows time series of model results (from the wind and pressure driven case) and observations that have been low-pass filtered with a cut-off period of 60 days. Clearly, the model is quite successful at capturing some of the low-pass variability seen in the sea level data, especially at Hampton Roads, but also at St. John's and Halifax. On the other hand, the discrepancy between model and data shows the influence of the seasonal steric signal, with observed sea level generally being higher than the model in the fall, and lower in the spring.

There are a number of reasons for expecting the model to perform better in regions with a large shelf width. In the first place, although we are using much higher resolution than in our previous studies, the model resolution (37 km in each direction at 34N) is not sufficient to resolve the shelf on most of the eastern boundary, or the narrow shelf offshore from Miami. In addition, our use of a barotropic model is strictly only valid in regions for which the shelf width is much greater than the internal radius of deformation (Huthnance, 1992). Although this is generally true along the western boundary, especially in the north (Middleton and Wright, 1991), it is unlikely to be valid on the eastern boundary, where the two length scales are of

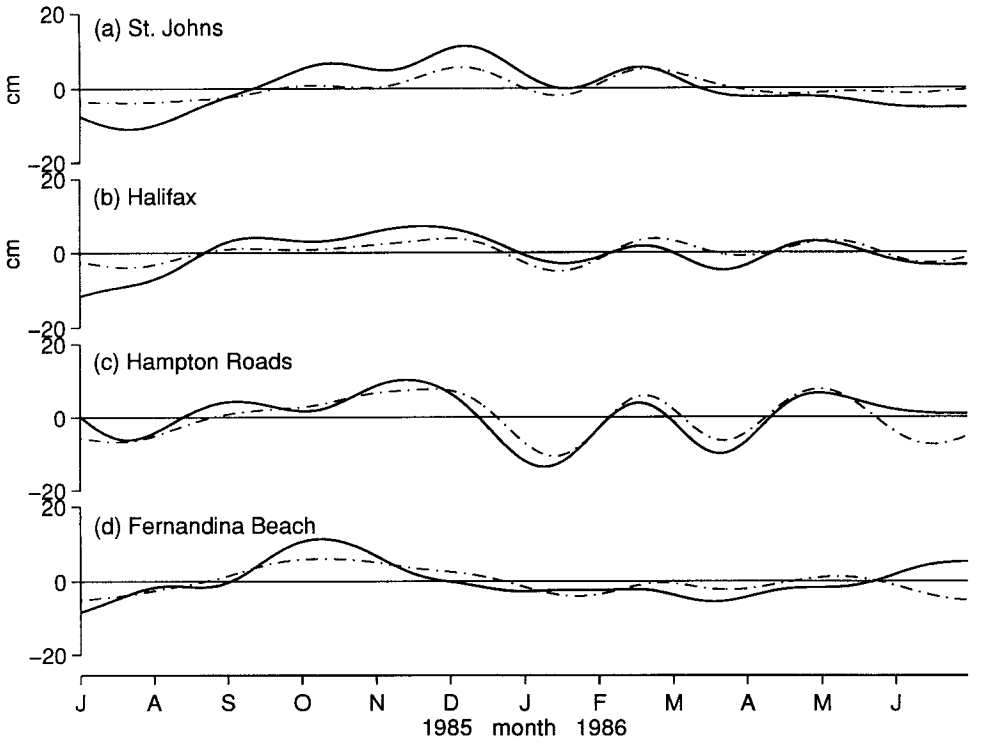

Figure 4. A comparison between low-pass filtered observations (solid line) and model results (dash-dot line) from the wind and pressure forced case. The cut-off period is 60 days.

similar order. Interestingly, it is also unlikely to be valid for the shelves around most of the North Pacific Ocean (an exception being along the coast of China). This could explain why Greatbatch and Goulding (1989b) were less successful in accounting for seasonal variations in sea level in the North Pacific, than they were in the North Atlantic. By contrast, Pares-Sierra and O'Brien (1989) showed that a reduced-gravity, shallow-water model is quite successful in capturing seasonal and interannual variations in sea level along the west coast of the United States, again pointing to the importance of baroclinic effects in regions with "narrow" shelves.

When comparing model results with observations, it should be remembered that there are errors in the 10 m wind and pressure fields used to drive the model. For example, the analysis procedure, used by ECMWF to produce the wind and pressure fields that are input to the model, was updated many times during the years 1985 and 1986 (see European Centre for Medium-Range Weather Forecasts, 1994). In addition, there were days when data were missing (see Table 3 in European Centre for Medium-Range Weather Forecasts, 1994). Errors also arise because the coarse resolution of the ECMWF data (2.5° × 2.5°) precludes inclusion of local effects near the tide gauges (e.g. neighboring topographic influences on the wind field). These

deficiencies undoubtedly contribute to the difference between model and observations.

The variance conserving spectra, shown in Figure 3, confirm the impression given by the time series plots of Figure 2 that the model underpredicts the response at the southern stations along the western boundary, but at high latitudes, notably St. John's and Halifax, the model does quite well. The pressure only case (the dashed line in Fig. 3) shows that pressure forcing generates little response in adjusted sea level. At Hampton Roads, the pressure and wind case (dashed-dot line) shows the broad peak seen in the data at periods of four to ten days, but with reduced amplitude. At Fernandina Beach, neither model case can account for the amplitude seen in the tide gauge data, although once again there is a peak in the same period range as found in the observations in the wind- and pressure-driven case (dashed-dot line).

Figure 5 shows plots of coherence squared and phase between model and observations. This shows the ability of the model to capture events in the observed time series. For the pressure and wind forced case (solid line), the coherence squared is high, above 0.5 for all the cases, reaching 0.75 at the northern stations. Phase is close to zero with relatively little variation over periods from 4–60 days. The pressure only case is barely able to yield significant coherence, further indication of the relative unimportance of pressure forcing.

We can also ask how well the model describes the coherence along the shelf. A comparison between two sets of stations, St. John's and Halifax (Fig. 6a) and Hampton Roads and Fernandina Beach (Fig. 6b), shows similar coherence squared and phase for both the model and observations, but with the model producing more coherence than the data. This is not surprising, given the smoothed model bottom topography, and the simplified nature of the model dynamics. At periods beyond five days, the variation of phase with period is consistent with shelf wave propagation. Similar results are obtained for other pairs of neighboring stations. Alongshelf coherence is considerably reduced as the station separation increases. This is a feature of both the model results and the observations. For example, comparing St. John's with those stations south of Halifax shows no significant coherence in either the data or the model.

Figure 7 shows plots of the model-computed root-mean-square variability. The plots are computed using unfiltered, adjusted sea level, sampled twice daily (recall that the forcing is provided by meteorological data sampled every 12 hours). These figures can be used as a guide in assessing the role of barotropic dynamics in contributing to sea-surface variability measured by satellite altimeters such as TOPEX/POSEIDON. The plot for the model run with wind forcing only (Fig. 7b) is quite similar to the wind and pressure forcing case (Fig. 7a), indicating the dominance of wind forcing in driving adjusted sea level over most of the model domain (Ponte, 1994). In Figure 7a, the greatest variability occurs over the shelves, especially

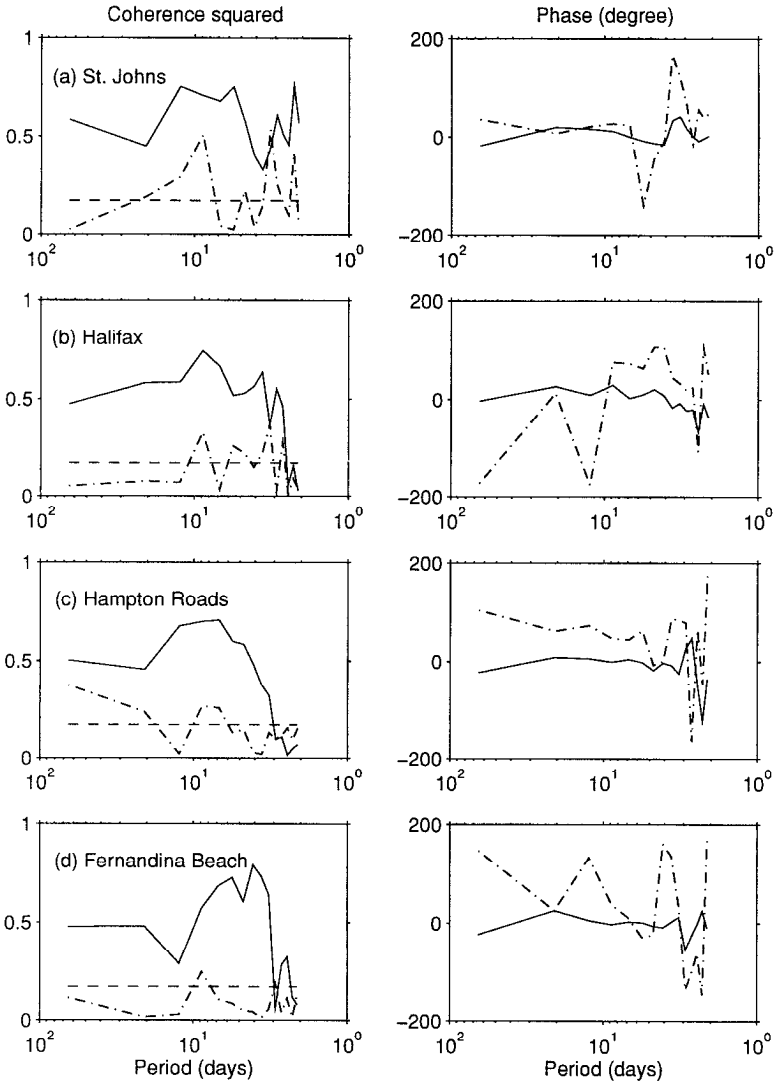

Figure 5. Coherence squared and phase between the model output and the data at (a) St. John's, (b) Halifax, (c) Hampton Roads and (d) Fernandina Beach. The solid line is the coherence between the observations and the model forced by wind and pressure. The dot-dashed line is between the observations and the model forced by pressure only. The 95% confidence limit for the coherence squared is shown as a horizontal dashed line. Positive phase means that the model leads the data.

the broad shelf from Hudson Bay to Florida on the western boundary, and on the Northwest European Shelf in the eastern Atlantic. The concentration of amplitude in the shelf regions is a consequence of a number of factors. For example, divergence of the wind-driven Ekman transport at the coast provides an important forcing term

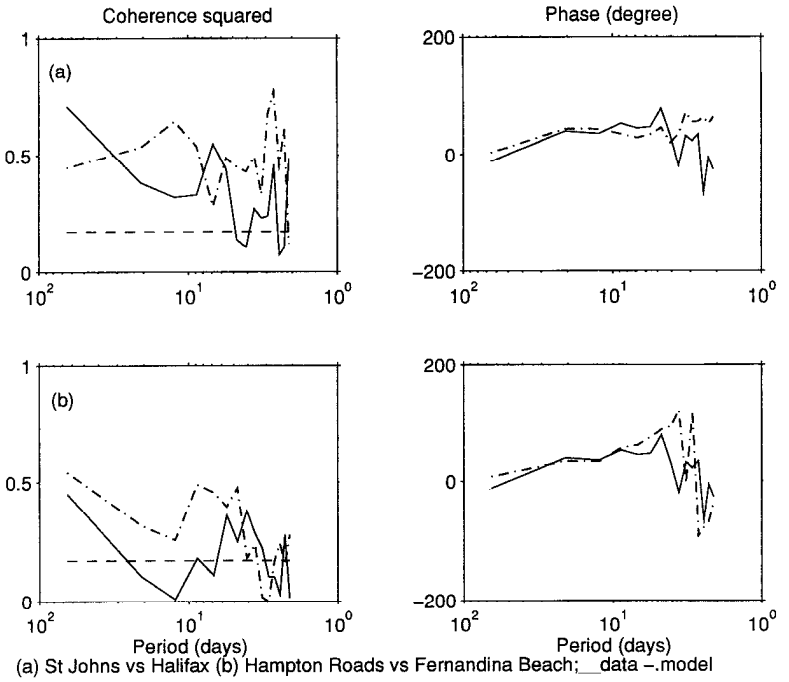

Figure 6. Coherence squared and phase between (a) St. John's and Halifax, and (b) Hampton Roads and Fernandina Beach, for the data (solid line) and the model (dot-dashed line). The 95% confidence limit for the coherence squared is shown as a horizontal dashed line. Positive phase means St. John's leads Halifax and Hampton Roads leads Fernandina Beach.

for topographic Rossby wave propagation on the shelf not available in the deep ocean. The shallow water depths also lead to stronger currents in shelf regions, with stronger geostrophic flows (e.g. alongshelf transport), in turn implying greater sea level variability than in deeper water. In the deep ocean, rms variability is greater in the northern part of the basin than farther south, a consequence of the stronger atmospheric forcing in the northern half associated with the North Atlantic storm tracks. Topographic Rossby waves also play a role in shaping the structure of the rms field. These waves propagate along f/H contours (Fig. 8), with large values of f/H to the right in the northern hemisphere. The influence of the f/H contours can be seen in Figures 7a,b. Note, for example, the southward tongue of increased variability over the Mid-Atlantic Ridge, associated with the southward dip of the f/H contours over the ridge. Also, the westward propagation of topographic waves increasingly concentrates the model response toward the west as the period increases, leading to greater rms variability on the western side of the basin.

Figure 7c shows rms adjusted sea level when the model is driven by atmospheric pressure forcing only. The relatively large amplitude in coastal seas, such as the North Sea and Hudson Bay, indicates a significant nonisostatic response (i.e.

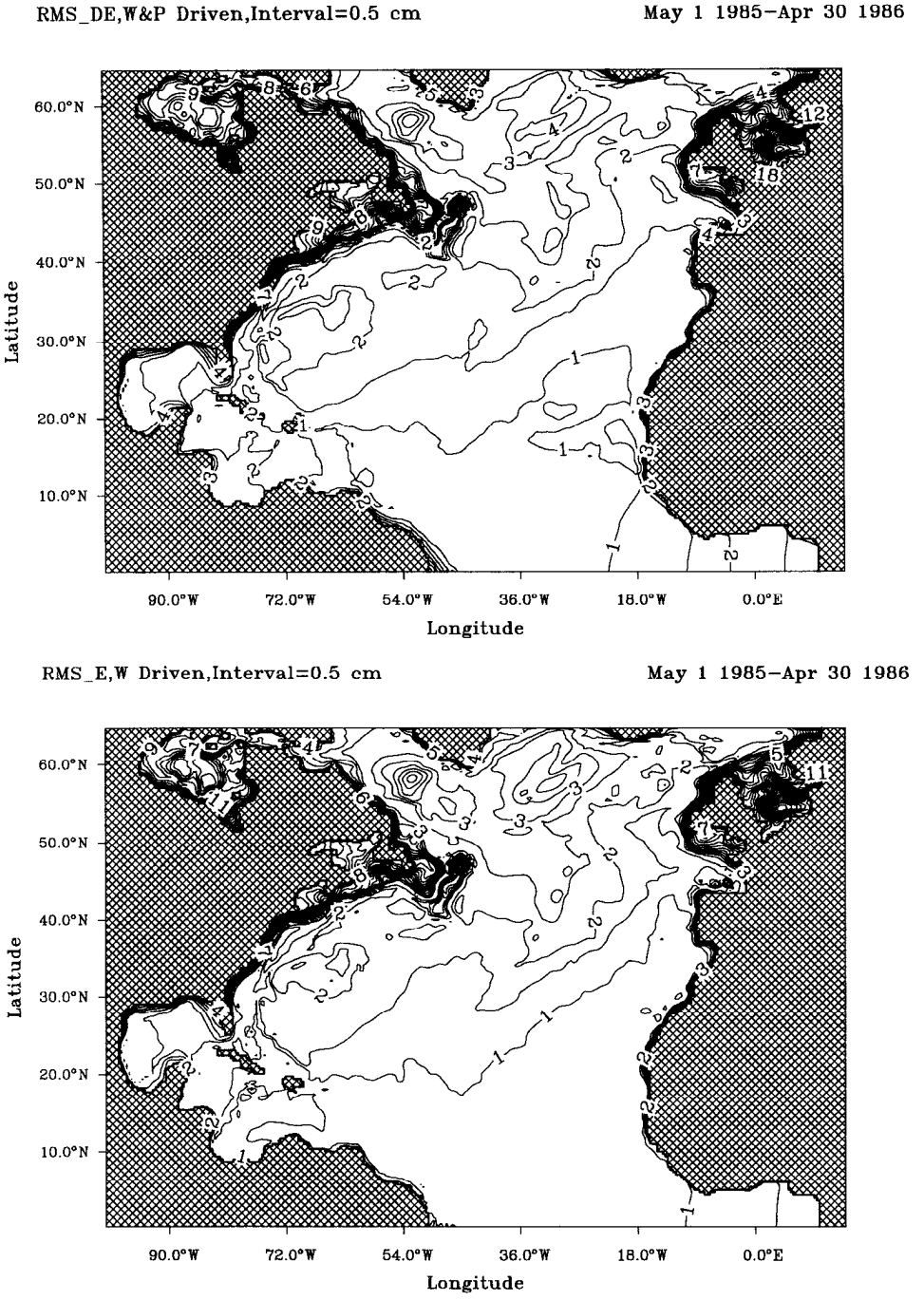

Figure 7. Root mean square adjusted sea level for three different model runs (a) wind and pressure forcing, (b) wind forcing only and (c) pressure forcing only. The plots are constructed using twice daily output from a one-year period, 1 May 1985 to 30 April 1986. The contour interval is 0.5 cm.

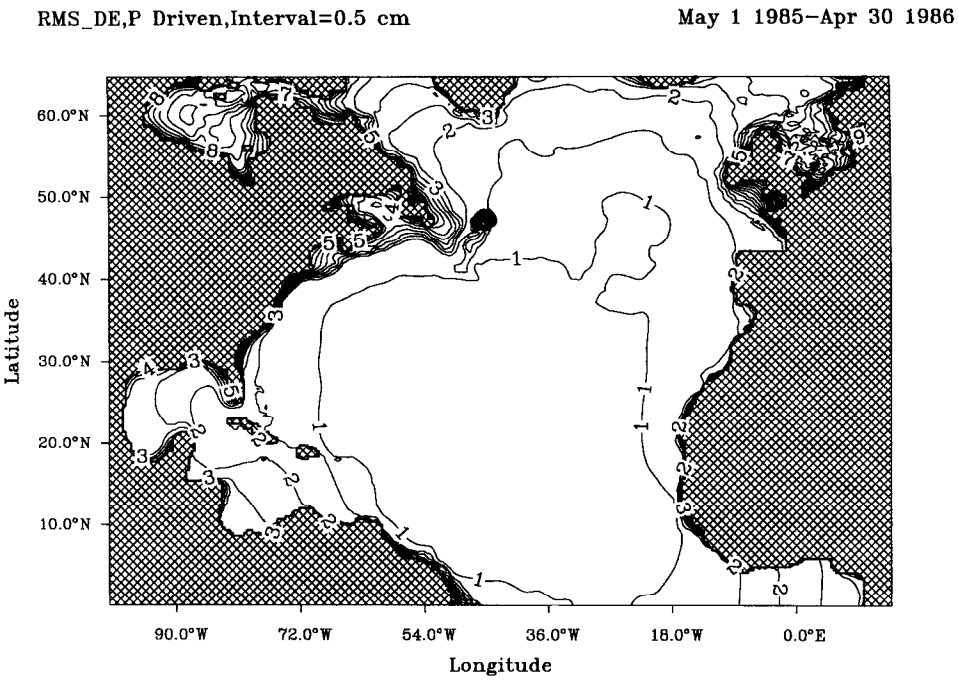

Figure 7. (Continued)

departure from the inverse barometer) in these regions and on the neighboring shelves. For example, Hudson Bay drives an important nonisostatic response on the northern Labrador shelf at time scales of two to six days, an effect that is captured by our model (de Young *et al.*, 1995), and has been discussed extensively by Wright *et al.* (1987). Ultimately, it is the shallow depth of Hudson Bay (and also the northwest European Shelf) that leads to the nonisostatic response in these regions. The adjustment to isostacy in response to atmospheric pressure forcing is accomplished by barotropic gravity waves (mostly coastal Kelvin waves) whose propagation speed, $(gH)^{1/2}$, is greatly reduced in semi-enclosed shallow sea regions, compared to the deep ocean. It follows that on the time scales considered (several days and greater), the inverse barometer is a good approximation in the deep ocean (Wunsch, 1972; Ponte *et al.*, 1991), but can break down in coastal regions, especially near to and downstream from (in the sense of long-topographic wave propagation) semi-enclosed, shallow seas such as Hudson Bay. There is a tendency in Figure 7c for rms variability to gradually decrease away from the coast into the interior of the basin. This is an indication of barotropic Kelvin waves propagating around the basin. These waves can also be excited by wind forcing (for example, in association with storm surges in the North Sea and elsewhere). It follows that wind forcing of these waves is likely to contribute to the large response on the shelves in Figure 7a,b.

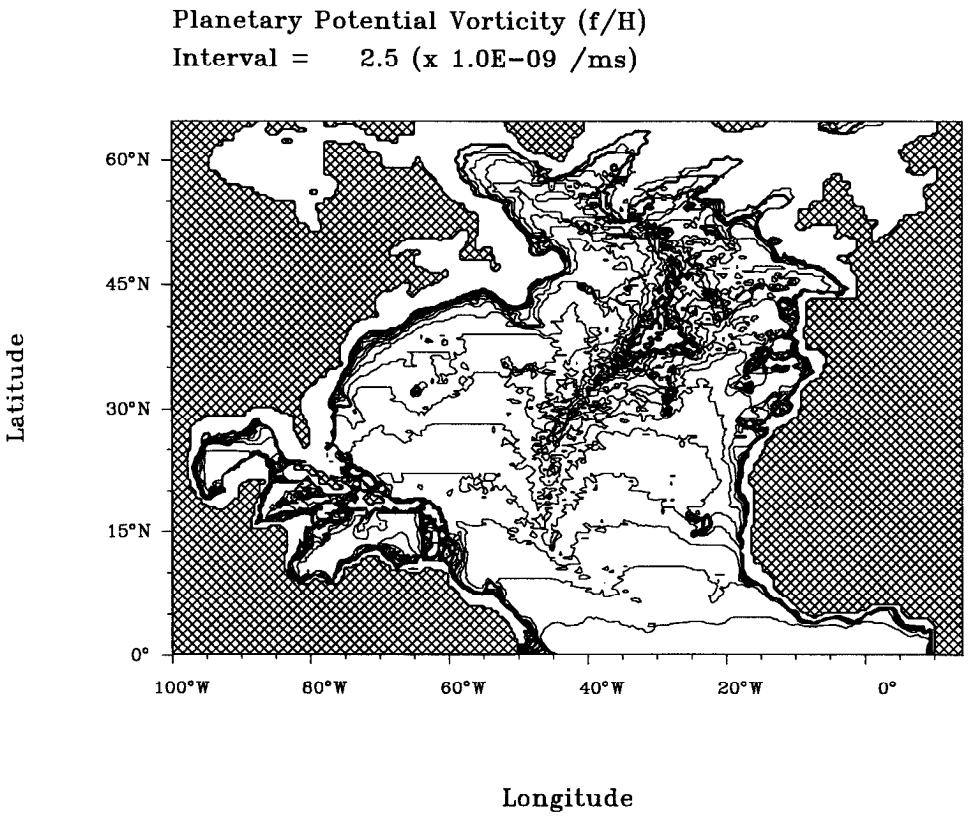

Figure 8. The f/H contours. The contour interval is 2.5×10^{-9} m^{-1} s^{-1}.

5. Summary

We have described results from a barotropic model, driven using forcing derived from ECMWF analyses of observed 10 m wind and atmospheric pressure data. The model has been used to study synoptic variability in adjusted sea level (that is with the inverse barometer removed) at coastal tide gauge stations around the North Atlantic. The model shows skill at explaining the observed sea level variations all along the western boundary from St. John's, Newfoundland, to Fernandina Beach, Florida. Coherence squared between model and data is in the range 0.5–0.75 over periods from three to ten days, with the phase close to zero. South of Cape Hatteras, the model underestimates the amplitude seen in the data, with much better agreement in amplitude north of the Cape. By contrast, the model does poorly at Haulover Pier, Miami, and on the eastern boundary of the North Atlantic. We attribute this partly to the inability of the model to adequately resolve the narrow shelf in these regions, and partly to the importance of baroclinic effects.

A possible reason for the poorer performance of the model south of Cape

Hatteras, compared to farther north, could be the presence of the Gulf Stream. Thompson (1986) noted a change in the character of monthly mean sea level north and south of the Cape. Another possibility is that our model may not adequately resolve the narrowing of the shelf at Cape Hatteras, and may not allow sufficient energy to pass southward beyond the Cape. Future work using higher resolution models, including the density stratification, and the offshore Gulf Stream, will be required to answer these questions.

Acknowledgments. We would like to thank K. Forward, A. Goulding, Y. Ren and T. Wareham for their computer assistance. We are grateful to P. Bolduc of the Marine Environmental Data Service (MEDS) in Ottawa, who provided the tide gauge data. Financial support was provided by NSERC in the form of Research Grants (BdeY and RJG), and as a Collaborative Special Projects (CSP) grant (RJG and BdeY) in support of Canadian University activities in the World Ocean Circulation Experiment (WOCE). Comments from reviewers led to improvements in the manuscript.

REFERENCES

Aikmann, F. *et al.* 1994. A coastal forecast system. The National Ocean Service/NOAA, Washington, D.C., 25 pp.

Akima, H. 1978. A method of bivariate interpolation and smooth surface fitting for irregularly distributed data points. ACM Trans. Math. Software, *4,* 148–159.

Blaha, J. 1984. Fluctuations of monthly mean sea level as related to the intensity of the Gulf Stream from Key West to Norfolk. J. Geophys. Res., *89*(C5), 8033–8042.

Blaha, J. and W. Sturges. 1987. Slope of sea level from Miami to Atlantic City. J. Phys. Oceanogr., *17,* 177–184.

Bryan, F. O. and W. R. Holland. 1989. A high resolution simulation of the wind- and thermohaline driven circulation in the North Atlantic Ocean, *in* Parameterization of Small-Scale Processes. Proc. 'Aha Huliko 'a Hawaiin Winter Workshop, P. Müller and D. Henderson, eds., University of Hawaii at Manoa, 99–115.

Bryan, K. 1969. A numerical method for the study of the circulation of the world ocean. J. Comp. Phys., *3,* 347–376.

Chase, R. R. P. 1979. The coastal longshore pressure gradient: Temporal variations and driving mechanisms. J. Geophys. Res., *84,* 4898–4904.

deYoung, B., R. J. Greatbatch, A. D. Goulding and K. Venguswamy. 1992. Bottom pressure variability on the Labrador Shelf: model-data comparisions. J Geophys. Res., *97,* 11,323–11,331.

deYoung, B., Y. Lu and R. J. Greatbatch. 1995. Synoptic bottom pressure variability on the Labrador and Newfoundland continental shelves. J. Geophys. Res., *100*(C5), 8,639–8,653.

European Centre For Medium-Range Weather Forcasts (ECMWF). 1994. The description of the ECMWF/WCRP Level III-A Global Atmospheric Data Archive, Technical Attachment, ECMWF, Shinfield Park, Reading, Berks, UK, 72 pp.

Ezer, T. and G. L. Mellor. 1994. Diagnostic and prognostic calculations of the North Atlantic circulation and sea level using a sigma coordinate ocean model. J. Geophys. Res., *99*(C7), 14,159–14,171.

Ezer, T., G. L. Mellor and R. J. Greatbatch. 1995. On the interpentadal variability of the North Atlantic Ocean: Model simulated changes in transport, meridional heat flux and coastal sea level between 1955–59 and 1970–74. J. Geophys. Res., *100*(C6), 10,559–10,566.

Fu, L.-L. *et al.* 1994. TOPEX/POSEIDON mission overview, J. Geophys. Res., *99*(C12), 24,369–24,382.

Garrett, C., F. Majaess and B. Toulany. 1985. Sea-level response at Nain, Labrador, to atmospheric pressure and wind. Atmosphere-Ocean, *23,* 95–117.

Gill, A. E. 1982. Atmosphere-Ocean Dynamics, Academic Press, New York, 662 pp.

Godin, G. 1972. The Analysis of Tides, University of Toronto Press, Toronto, 264 pp.

Greatbatch, R. J., B. deYoung, A. Goulding and J. Craig. 1990. On the influence of local and North Atlantic wind forcing on the seasonal variation of sea level on the Newfoundland and Labrador shelf. J. Geophys. Res., *95,* 5,279–5,289.

Greatbatch, R. J. and A. Goulding, 1989a. Seasonal variations in a linear barotropic model of the North Atlantic driven by the Hellerman Rosenstein wind stress field. J. Phys. Oceanogr., *19,* 572–595.

—— 1989b. Seasonal variations in a linear barotropic model of the North Pacific driven by the Hellerman Rosenstein wind stress field, J. Geophys. Res., *94*(C9), 12,645–12,665.

Greatbatch, R. J., Y. Lu, B. deYoung and J. C. Larsen. 1995. The variation of transport through the Straits of Florida: A barotropic model study, J. Phys. Oceanogr., *25,* 2726–2740.

Heaps, N. S. 1971. On the numerical solution of the three-dimensional hydrodynamical equations for tides and storm surges. Mémoires Société Royale des Sciences de Liège, *I,* 143–180.

Huthnance, J. M. 1992. Extensive slope currents and the ocean-shelf boundary. Prog. Oceanogr., *29,* 161–196.

Large, W. G. and S. Pond. 1981. Open ocean momentum flux measurements in moderate strong winds. J. Phys. Oceanogr., *11,* 324–336.

Maul, G. A., D. A. Mayer and M. Bushnell. 1990. Statistical relationships between local sea level and weather with Florida-Bahamas cable and Pegasus measurements of Florida Current volume transport. J. Geophys. Res., *95,* 3287–3296.

Middleton, J. F. and D. G. Wright. 1991. Coastal-trapped waves on the Labrador Shelf, J. Geophys. Res., *96,* 2599–2617.

Noble, M. and B. Butman. 1979. Low-frequency wind-induced sea level oscillations along the east coast of North America. J. Geophys. Res., *84,* 3227–3236.

Pares-Sierra, A. and J. J. O'Brien. 1989. The seasonal and interannual variability of the California Current system: A numerical model, J. Geophys. Res., *94*(C3), 3159–3180.

Pattullo, J., W. Munk, R. Revelle and E. Strong. 1955. The seasonal oscillation of sea level. J. Mar. Res., *14,* 88–156.

Ponte, R. M. 1994. Understanding the relationship between wind- and pressure-driven sea level variability. J. Geophys. Res., *99,* 8033–8040.

Ponte, R. M., D. A. Salstein and R. D. Rosen. 1991. Sea level response to pressure forcing in a barotropic numerical model. J. Phys. Oceanogr., *21,* 1043–1057.

Sandstrom, H. 1980. On the wind-induced sea level changes on the Scotian Shelf. J. Geophys. Res., *85*(C1), 461–468.

Sturges, W. 1974. Slope of sea level along continental boundaries. J. Geophys. Res., *79,* 825–830.

Thompson, K. R. 1986. North Atlantic sea-level and circulation. Geophys. J. Royal Astron. Soc., *87,* 15–32.

Thompson, K. R., J. R. N. Lazier and B. Taylor. 1986. Wind-forced changes in Labrador Current transport. J. Geophys. Res., *91,* 14261–14268.

Wang, D. P. 1979. Low frequency sea level variability on the Middle Atlantic Bight. J. Mar. Res., *37,* 683–707.

Wright, D. G., D. A. Greenberg and F. G. Majaess. 1987. The influence of bays on adjusted sea level over adjacent shelves with application to the Labrador Shelf. J. Geophys. Res., *92,* 14610–14620.

Wunsch, C. 1972. Bermuda sea level relation to tides, weather and baroclinic fluctuations. Rev. Geophys., *10,* 1–49.

—— 1991a. Global-scale sea surface variability from combined altimetric and tide-gauge measurements. J. Geophys. Res., *96*(C8), 15,053–15,082.

—— 1991b. Large-scale response of the ocean to atmospheric forcing at low frequencies. J. Geophys. Res., *96*(C8), 15,083–15,092.

Received: *6 April, 1995;* revised: *14 November, 1995.*